cancers

MDPI

Article

A Novel Mouse Model to Identify Antigen-Specific Immune Responses in Pancreatic Cancer Cachexia

Ayushi Das [1,2,†], Debasmita Mukherjee [1,2,†], Liliana D'Alesio [1], Jessica Wedig [1,2], Hannah Lathrop [1], Maria Schmidt [1], Abigail Guenther [1], Morgan Kaiser [1], Jeon Varghese [1], Bryan Remaily [3], Samuel K. Kulp [3], Jeovanna Lowe [4], Jill A. Rafael-Fortney [4], Justin Thomas [3], Kyeongmin Kim [3], Adeoluwa Adeluola [3], Stacey Culp [5], Andrew Gunderson [6], Mitch A. Phelps [3], Christopher C. Coss [3] and Thomas A. Mace [1,7,*]

[1] The James Comprehensive Cancer Center, The Ohio State University Wexner Medical Center, Columbus, OH 43210, USA; ayushi.das@osumc.edu (A.D.); lathrop.41@buckeyemail.osu.edu (H.L.); abigail.guenther@osumc.edu (A.G.); varghese.102@buckeyemail.osu.edu (J.V.)
[2] Molecular, Cellular and Developmental Biology Program, The Ohio State University, Columbus, OH 43210, USA
[3] Division of Pharmaceutics and Pharmacology, College of Pharmacy, The Ohio State University, Columbus, OH 43210, USA
[4] Department of Physiology and Cell Biology, College of Medicine, The Ohio State University, Columbus, OH 43210, USA
[5] Department of Biomedical Informatics, The Ohio State University, Columbus, OH 43210, USA
[6] Department of Surgical Oncology, The Ohio State University, Columbus, OH 43210, USA
[7] Division of Gastroenterology, Hepatology, and Nutrition, Department of Internal Medicine, The Ohio State University Wexner Medical Center, Columbus, OH 43210, USA
* Correspondence: thomas.mace@osumc.edu; Tel.: +1-(614)-366-3247
† These authors contributed equally to this work.

Simple Summary

Pancreatic Ductal Adenocarcinoma (PDAC) is frequently complicated by cachexia, a serious condition in which patients involuntarily lose body weight due to skeletal muscle wasting and fat loss. Cachexia influences anti-tumor immune responses and hinders therapeutic success in several cancers. However, the mechanisms underlying crosstalk between cachexia and the immune system in PDAC are poorly understood, underscoring an urgent need for further investigations in novel preclinical models. Here, we report a novel orthotopic pancreatic cancer cachexia model in C57BL/6J mice. We conclude that this mouse model recapitulates clinically relevant hallmarks of cachexia, defined by decrease in body weight, fat loss, systemic inflammation and skeletal muscle wasting, thereby providing a robust system for investigating antigen-specific T cell responses in the cachectic background. By elaborating the complex interplay between cachexia and immunomodulation, this model will enable preclinical evaluation of diverse immunotherapies, significantly advancing the search for effective treatment of PDAC patients with cachexia.

Check for updates

Academic Editor: Jelena Grahovac

Received: 22 December 2025
Revised: 30 January 2026
Accepted: 2 February 2026
Published: 11 February 2026

Copyright: © 2026 by the authors. Licensee MDPI, Basel, Switzerland. This article is an open access article distributed under the terms and conditions of the Creative Commons Attribution (CC BY) license.

Abstract

Background: Pancreatic Ductal Adenocarcinoma (PDAC) has a dismal five-year survival rate of 13% and is closely associated with cachexia. Cancer cachexia is a multifactorial syndrome characterized by irreversible wasting of skeletal muscles, fat loss and systemic inflammation. While cachexia is known to confer resistance to immune checkpoint inhibition in several cancers, the bidirectional relationship between cachexia and the immune system in PDAC remains unclear, necessitating the development of novel preclinical models. Our laboratory has characterized a novel pancreatic cancer cachexia model in C57BL/6J mice by utilizing the pancreatic cancer cell line called KPCL-4 derived from KPC-LSIY mice

(*Kras*$^{LSL\text{-}G12D/+}$*Tp53*$^{LSL\text{-}R172H/+}$ *Pdx1-Cre/R26*$^{LSL\text{-}LSIY}$). Methods: KPCL-4 cells were orthotopically injected into the pancreas of male and female C57BL/6J mice and hallmarks of cachexia were assessed at endpoint by measurement of tumor weight, terminal tumor-adjusted body weight, skeletal muscle, adipose tissue, liver and spleen masses, proteolytic markers and grip strength. Plasma cytokine and chemokine concentrations were quantified by Luminex assay and high-dimensional flow cytometry was used to investigate changes in tumor-infiltrating immune populations. Results: We observed a sex bias in cachexia presentation despite similar tumor weights in male and female mice, whereby males exhibited a >5% decrease in terminal tumor-adjusted body weight ($p < 0.001$), >50% fat loss ($p < 0.001$), upregulation of proteolytic markers in skeletal muscles ($p < 0.01$) and reduction in skeletal muscle mass ($p < 0.05$), function ($p < 0.01$) and cross-sectional area ($p < 0.0001$) whereas females demonstrated conserved skeletal muscle mass with 33% fat loss ($p < 0.05$), reduction in muscle cross-sectional area ($p < 0.0001$) and splenomegaly ($p < 0.01$). While intra-tumoral immune populations did not exhibit sex-specific differences, plasma cytokine concentrations were differentially upregulated in males and females, suggesting functional differences in immune cells as potent drivers of sex bias in KPCL-4-driven cachexia. Conclusions: The KPCL-4 orthotopic PDAC model exhibits prominent hallmarks of cachexia and serves as a novel platform for investigating the complex interplay between cancer cachexia and immunomodulation.

Keywords: Immunotherapy; immunomodulation; pancreatic cancer; cachexia; preclinical models

1. Introduction

Cachexia is a multifactorial systemic disorder that is characterized by involuntary loss of body weight due to progressive wasting of skeletal muscles and adipose tissue [1,2]. Often associated with chronic diseases like cancer, cachexia management presents an unmet clinical need as it cannot be reversed with standard nutritional interventions and ultimately worsens the prognosis of the primary disease [1]. It has the highest prevalence in gastrointestinal malignancies, particularly in pancreatic ductal adenocarcinoma (PDAC), affecting more than 80% patients and contributing to one third of pancreatic cancer deaths [3–5]. Currently, the lack of effective early detection of PDAC results in disease progression to advanced stages where the aggressive and immunosuppressive pancreatic tumor microenvironment (TME), in combination with cachexia, significantly enhances the morbidity of the disease.

Sex has been known to play a role in altered disease manifestation for multiple diseases including cancer. In patients with pancreatic cancer, there is evidence of sexual dimorphism where low skeletal muscle mass and loss of body weight is observed in males specifically [6,7]. Female patients, on the other hand, have been observed to demonstrate low subcutaneous and visceral adipose tissue with weight loss instead [6]. Recently, preclinical investigations have started delving into functionally understanding the sex bias in cachexia in animal models of various cancers. For instance, in the commonly studied C26 colon cancer cachexia model, female mice display many common characteristics of cachexia such as fat loss, hepatosplenomegaly and upregulation of muscle-associated proteolytic markers despite relatively preserved skeletal muscle mass in early-stage cachexia compared with males [8]. Another investigation has reported that differential dependency of IL-6, in a sex-specific manner, drives the severe cachectic phenotype in males [9]. These studies highlight the need to build and study preclinical models of pancreatic cancer cachexia that

will provide insight into the differential biology of cachexia development in males and females and allow for development of tailored therapeutics.

It is now widely recognized that there is a significant tumor-organ and immune-cell crosstalk involved in the development and progression of cancer cachexia. A recent investigation in a KPC-derived orthotopic PDAC mouse model reported that tumor-infiltrating macrophages induce the secretion of TNF superfamily cytokines from tumor cells, which in turn, promote skeletal muscle wasting via the activation of Fbxo32 (Atrogin-1) and Trim63 (MuRF1) [10]. Similarly, research in a pre-cachectic autochthonous PDAC mouse model demonstrated that tumor-induced IL-6 expression triggers a systemic metabolic stress response, which suppresses multiple intra-tumoral immune pathways and antagonizes immune checkpoint inhibition [11]. Furthermore, owing to the sensitivity of T cells to local metabolic changes, the potential of cachexia to suppress anti-tumor T cell responses is gaining attention and can have tremendous implications in governing the efficacy of immune-based therapies [11–13].

Immune checkpoint inhibition (ICI) has revolutionized the landscape of cancer therapies. However, despite promising outcomes in several solid tumors such as lung cancer and melanoma, ICI remains ineffective in pancreatic cancer [14–16]. The systemic inflammation and metabolic alterations associated with cachexia potentially suppresses anti-tumor immune responses, reducing the effectiveness of immune checkpoint inhibitors. Although the role of cachexia in influencing a therapeutic response in pancreatic cancer has not been directly investigated, recent research in other cancers has revealed that cachexia plays a pivotal role in determining patient response to anti-cancer therapies. A retrospective analysis of patients with advanced non-small cell lung cancer (NSCLC) receiving PD-1/PD-L1 inhibitors established that cachexia is associated with shorter progression-free survival and overall worse prognosis, regardless of tumor PD-L1 expression, suggesting that the presence of cachexia can serve as an independent prognostic factor for predicting ICI success in these patients [17,18]. These results are well complemented by other studies in the C26 and LLC tumor models of cachexia which demonstrated that tumor-bearing, cachectic mice had a significantly higher clearance of the PD-1 inhibitor, pembrolizumab, compared with tumor-free mice without cachexia, rendering cachectic mice unresponsive to PD-1 inhibition [19]. These observations suggest the possibility of direct crosstalk between immune cells and cachectic drivers, underscoring the need for mechanistic investigations in preclinical pancreatic cancer models capable of studying cachexia from an immunological perspective.

In this study, we have utilized the KPCL-4 cell line (previously described as PK5L1948) to study the pancreatic tumor-specific expression of the model antigen SIYRYYGL (SIY) in the context of cachexia [20]. The KPCL-4 cell line provides a convenient way of permitting orthotopic implantation in mice to understand pancreatic disease biology and has the potential to be a valuable resource for detecting tumor antigen-specific immune cell responses in the pancreatic TME. Here, we demonstrate that the KPCL-4 orthotopic model of pancreatic cancer can show sex-specific differences in cachexia development and can serve as an effective preclinical model for future studies investigating mechanisms by which cachexia impacts immunotherapy responses in pancreatic cancer.

2. Methods

2.1. Reagents and Cell Culture

The KPCL-4 cell line, expressing the SIYRYYGL (SIY) antigen, was obtained from Dr. Andrew Gunderson. It is derived from KPC-LSIY mice which were generated by crossbreeding *Pdx1-Cre/R26*$^{LSL\text{-}LSIY}$ with *Kras*$^{LSL\text{-}G12D/+}$*Tp53*$^{LSL\text{-}R172H/+}$—mice [20]. KPCL-4 cells were grown in RPMI medium (Fisher Scientific Waltham, MA, USA) supplemented with

10% fetal bovine serum (FBS; Biowest, Riverside, MO, USA) and 1% penicillin-streptomycin at 37 °C in a humidified chamber with 5% CO_2. Cells were suspended in Corning™ Matrigel™ GFR Membrane Matrix (Fisher Scientific) for orthotopic injection.

2.2. Mice

All animal studies were conducted according to protocols approved by The Ohio State University Institutional Animal Care and Use Committee. Age-matched male and female C57BL/6J mice (Jackson Laboratories, Bar Harbor, ME, USA) were under constant photoperiod conditions (12 h light/12 h dark) and had ad libitum access to water and a standard diet. Mice were group-housed to avoid confounding effects of social isolation stress, which is known to alter metabolism, immune responses, tumor progression and body weight in murine models [21,22]. For the experiment, male and female mice aged 8 to 10 weeks were randomly assigned to tumor-free (TF) or KPCL-4 tumor-bearing (TB) groups, with 10 mice per group unless otherwise stated. Mice were injected with 50 µL of either PBS (TF) or 0.5×10^5 KPCL-4 cells (TB) into the distal end of the pancreas in a 1:1 Matrigel mixture. Specific details on orthotopic surgery are provided below in Section 2.3. Mouse body weights were recorded throughout the study. Forelimb grip strength of mice across experimental groups were measured using an inclined grip strength meter (Harvard Bioscience, Holliston, MA, USA) in the first week post injection (initial) and at endpoint. Mice were euthanized by CO_2 inhalation and exsanguination via cardiac puncture 21 days post tumor implantation (in accordance with institutional guidelines for animal care and our animal protocol approved by the Institutional Animal Care and Use Committee (IACUC) at The Ohio State University; 2009A0178-R5). Following euthanasia, the tumor, serum, left hind limb skeletal muscles (gastrocnemius, quadricep and tibialis anterior), visceral fat (gonadal adipose tissue), liver and spleen were excised for weighing and other analyses. Terminal tumor-adjusted body weights were determined by subtracting the weight of the excised tumor from the total body weight of the mouse at the end of the study. The % weight change in mice was calculated as: ((Initial body weight prior to injection–terminal tumor-adjusted body weight at endpoint)/Initial body weight prior to injection)) ×100. The %change in grip strength per mouse was calculated as: ((Initial grip strength–Grip strength at endpoint)/Initial grip strength)) × 100.

2.3. Orthotopic Surgery

Mice were administered with the slow-release analgesic Buprenorphine prior to surgery. For surgery, mice were anesthetized with isoflurane on the operating table. After cleaning the incision area (~1.5 cm left of the abdominal midline) with 70% ethanol and chlorhexidine, a small longitudinal incision (approximately 0.5 cm) was made through the skin and peritoneum to access the abdominal cavity. The spleen was located with forceps and a cotton-tipped applicator was used to gently roll it outward to expose the adjacently located pancreas without direct contact. Then, 0.5×10^5 KPCL-4 cells (in 1:1 Matrigel mixture) or PBS were injected into the distal end of the pancreas of experimental and sham mice respectively using a 1 mL BD® Tuberculin Syringe with Detachable 27 G × 1/2 in Needle (Fisher Scientific). After injection, the syringe was held in the pancreas for 30 s to minimize chances of leakage before returning the spleen and pancreas to the abdominal cavity. Finally, the peritoneal and skin layers were aligned, and the incision was closed using 9 mm EZ Clip surgical staple wound clips (Braintree Scientific, Braintree, MA, USA). Post-operatively, mice were placed on a heating pad for thermal support and monitored closely for signs of distress.

2.4. Randomization and Blinding Procedures

All animal studies were conducted according to protocols approved by The Ohio State University. Mice were randomized at the time of cage allocation using a stratified randomization approach. Specifically, male and female mice were stratified by body weight and then randomly allocated to tumor-free (TF) or KPCL-4 tumor-bearing (TB) groups, with up to 5 animals of the same experimental group per cage. Mice in each experimental group as well as cages were assigned unique identification numbers at the beginning of the study and were concealed from primary investigators to facilitate de-identification. Consequently, investigators performing longitudinal body weight measurements, functional assessments (grip strength, food consumption), necropsy and immunofluorescence-based muscle atrophy evaluation were blinded to the experimental groups throughout the duration of the study. Group allocations were revealed after data collection to ensure unbiased assessments.

2.5. Muscle Cross-Sectional Area Measurement

Frozen muscles were cryo-sectioned to a thickness of 8 µm and collected on Superfrost Plus slides (Thermo Fisher Scientific, Waltham, MA, USA). Sections were stained with hematoxylin and eosin by standard methods to assess overall histology. For immunofluorescence, muscle sections were hydrated in PBS for 15 min, blocked with 5% non-fat dry milk in PBS (Bio-Rad, Hercules, CA, USA) for 1 h, and then washed 3 times with PBS at room temperature. Subsequently, primary antibody (rat anti-laminin-2; Sigma-Aldrich, St. Louis, MO, USA) was added to the sections at a dilution of 1:500 in blocking solution and incubated overnight at 4 °C. Slides were rinsed thrice with PBS, followed by four additional 15 min PBS washes at room temperature to ensure removal of unbound antibodies. Next, sections were incubated with the secondary antibody (goat anti-rat-594; Invitrogen, Carlsbad, CA, USA) at a 1:200 dilution in blocking solution for 1 h in the dark, at room temperature. Following PBS washes, sections were incubated for 10 min with DAPI (Sigma-Aldrich) and again washed 3 times with PBS. Sections were mounted with ProLong Gold mounting media (Invitrogen) and 1.5 mm cover slips. Slides were imaged using a 20× objective on a Nikon NiE microscope equipped with a Moment CMOS camera and Nikon Elements software v6.10.03 (Nikon, Melville, NY, USA). All cross-sectional areas (CSA's) imaging and analysis were blinded. The CSA of each muscle section was quantified using the Imaris image software v10.1.1 (Oxford Instruments, Abingdon, UK) as described previously to obtain muscle fiber cross-sectional area measurements [23].

2.6. Gene Expression Analyses by Real-Time Quantitative Reverse Transcription PCR (RT-qPCR)

After euthanasia, quadriceps tissue was snap-frozen in liquid nitrogen and stored at −80 °C until analysis of *Trim63* and *Fbxo32* expression. For RNA extraction, 25–30 mg tissue was lysed and homogenized in 1 mL TRIzol™ Reagent (Thermo Fisher) and further processed according to TRIzol™ manufacturer's instructions. 1500 ng of RNA was used to make cDNA by SuperScript™ III First-Strand Synthesis System (Thermo Fisher Scientific). Real-time quantitative PCR (RT-qPCR) was then performed using specific primers for *Fbxo32* (Forward primer: TTCAGCAGCCTGAACTACGA, Reverse primer: AGTATCCATGGCGCTCCTTC) and *Trim63* (Forward primer: GTGACCAAGGAGAATAGCCAC, Reverse primer: ATCAGAGCCTCGATGAAGCC) [19,24]. *Gapdh* was used as an internal control gene (Forward primer: GGGTTCCTATAAATACGGACTGC, Reverse primer: TACGGCCAAATCCGTTCACA) [25]. RT-qPCR reactions were conducted on the QuantStudio 7 system (Applied Biosystems, Foster City, CA, USA) using the Fast SYBR Green Master Mix (Applied Biosystems).

2.7. Isolation of Tumor-Infiltrating Lymphocytes (TILs)

Tumor tissue was cut into small pieces (~0.15–0.20 g) and incubated in 3 mL PBS containing 20 µg/mL Liberase™ TL (Sigma-Aldrich) on ice. Following a brief mechanical agitation in the GentleMACS Tissue Dissociator (Miltenyi Biotec, Gaithersburg, MD, USA), the tissue was incubated in the New Brunswick I24 Incubator Shaker (New Brunswick Scientific, Edison, NJ, USA) at 37 °C for 30 min. The digested tissue was passed through a 70 µm cell strainer, rinsed with 1X PBS and centrifuged at 500× *g* for 5 min. The supernatant was discarded and the cell pellet was resuspended in residual volume for red blood cell lysis. Red blood cells were lysed using 10 mL 1X red blood cell lysis buffer (8.26 g Ammonium Chloride, 1 g Potassium Bicarbonate and 0.037 g EDTA in 1 L diH_2O) for two minutes at room temperature, which was then neutralized with 40 mL PBS and centrifuged at 500× *g* for 5 min. The supernatant was discarded and cells were resuspended in freezing media (90% FBS + 10% DMSO) for storage at −80 °C until analysis.

2.8. Flow Cytometry

TILs were thawed and incubated with the viability dye (Live/Dead-440UV; BD Bioscience, Franklin Lakes, NJ, USA) for 15 min at room temperature, protected from light. Cells were then washed with FACS buffer (5% FBS in 1X PBS) before addition of the SIY tetramer-AlexaFluor 647 (clone: H-2kb, NIH Tetramer Core Facility, Emory University, Atlanta, GA, USA). After a 30 min incubation with the tetramer in the dark at room temperature, cells were washed with FACS buffer, and Fc receptors were blocked using the TruStain FcX™ PLUS Antibody (anti-mouse CD16/32; Biolegend, San Diego, CA, USA). Next, cells were stained with appropriate surface-stain antibodies for 30 min on ice, protected from light. For staining intracellular immune markers, surface-stained cells were washed and permeabilized for 30 min on ice using eBioscience™ Foxp3/Transcription Factor Staining Buffer Set (Fisher Scientific) in the dark before a 30 min incubation with the respective antibodies at room temperature. Subsequently, cells were fixed in 1% Formalin and run on the 5-laser Cytek Aurora™ system (Cytek Bioscience, Fremont, CA, USA). FCS data analysis and quantification were performed using the OMIQ software (https://www.omiq.ai/; accessed on 1 June 2024 and 1 January 2026; Dotmatics, Boston, MA, USA). Antibodies used for staining are listed in Table 1.

Table 1. Antibodies used for TIL and splenocyte staining.

Marker	Fluor	Clone	Catalogue
CD45	BUV805	30-F11	BD Bioscience; 568,336
CD19	BUV737	1D3	BD Bioscience; 612,781
CD3	BV786	17A2	BD Bioscience; 564,010
NK1.1	RB780	PK136	BD Bioscience; 569,231
CD4	BV510	RM4-5	BD Bioscience; 563,106
CD8	APC-Cy7	53–6.7	BD Bioscience; 561,967
CD44	BUV496	IM7	BD Bioscience; 741,057
CD62L	BV421	MEL-14	BD Bioscience; 562,910
TIM-3	PE-CF594	5D12/TIM-3	BD Bioscience; 566,998
PD-1	RY586	J43	BD Bioscience; 753,837
TCF-1	Alexa-fluor 488	S33-966	BD Bioscience; 567,018
CD11c	BUV615	HL3	BD Bioscience; 751,265

Table 1. *Cont.*

Marker	Fluor	Clone	Catalogue
CD11b	BB700	M1/70	BD Bioscience; 566,416
F4/80	R718	T45-2342	BD Bioscience; 752,152
CD206	BUV395	Y17-505	BD Bioscience; 568,817
Ly6-G	BV711	1A8	BD Bioscience; 563,979
Ly6-C	PacBlue	HK1.4	BD Bioscience; 128,014

2.9. Plasma Cytokine Analysis

Whole blood was collected via cardiac puncture into heparinized tubes (BD Microtainer, PST Tubes, Becton, Dickinson and Company, Franklin Lakes, NJ, USA) at endpoint and maintained at room temperature. The samples were then centrifuged at 10,000× *g* for 2 min to remove cells and platelets. The supernatant (plasma) was transferred to fresh tubes and stored at −80 °C until analysis. For cytokine analysis, plasma from each mouse was diluted 1:1 in PBS (PH ~7.5) and shipped to Eve Technologies Corporation (Calgary, AB, Canada). Terminal plasma cytokine and chemokine levels were measured with Mouse Cytokine/Chemokine 32-Plex Discovery Assay® Array (MD32, Eve Technologies). The multiplex analysis was performed using the Luminex® 200™ system (Luminex Corporation, DiaSorin, Saluggia, Italy) with Bio-Plex Manager™ software (Bio-Rad Laboratories Inc., Hercules, CA, USA). Assay sensitivities of these markers range from 0.3 to 30.6 pg/mL. Results that were out of range (relative to the standard curve) were excluded prior to analysis.

2.10. Statistics

Group means with error bars were plotted for MTF, MTB, FTF, and FTB groups for all quantitative outcomes using GraphPad Prism v10.3.1. Kruskal–Wallis tests were used to compare all four groups, while Mann–Whitney U tests were used for pairwise comparisons. The level of significance was $\alpha = 0.05$ for all tests. For analyzing muscle fiber cross-sectional areas, the Vargha-Delaney A-statistics of the muscle fiber cross-sectional areas between TB and TF mice was calculated and the difference was tested by Brunner–Munzel test using R Studio v4.3.2 (R Core Team, Vienna, Austria) [23].

3. Results

3.1. Orthotopic Pancreatic Implantation of KPCL-4 Cells Results in Weight Loss and Muscle Weakness in Tumor-Bearing Mice

Cachexia is primarily characterized by unintentional and irreversible loss of body weight and muscle mass, resulting in overall weakness and fatigue in affected individuals [1,2]. To assess the cachectic potential of KPCL-4 cells, we injected this murine pancreatic cancer cell line into the pancreas of male and female C57BL/6J mice ($n = 10$/group) and evaluated the endpoint tumor weight, change in body weight and grip strength. At the study endpoint, the excised tumor weights did not show any significant difference between male (MTB) and female (FTB) tumor-bearing groups (Figure 1A). However, both MTB and FTB mice demonstrated at least a 5% reduction in the terminal tumor-adjusted body weight compared to the corresponding tumor-free mice (MTF or FTF, respectively), with the weight loss in males being two-fold higher relative to females (Figure 1B), indicating a sex bias in cachexia presentation. The average food intake per cage of MTB and FTB mice did not show any significant reduction relative to the respective tumor-free (MTF and FTF) mice throughout the study timeline, suggesting that the KPCL-4 tumor induces weight loss via metabolic reprogramming and hypercatabolism rather than loss of appetite

(Supplementary Figure S1). Further, to understand the functional implications of loss of body weight, we measured the forelimb grip strength of these mice at two different time points throughout the study timeline and observed that MTB mice demonstrate a sustained loss of grip strength of 26.3% relative to the MTF controls whereas FTB mice retained their grip strength (Figure 1C).

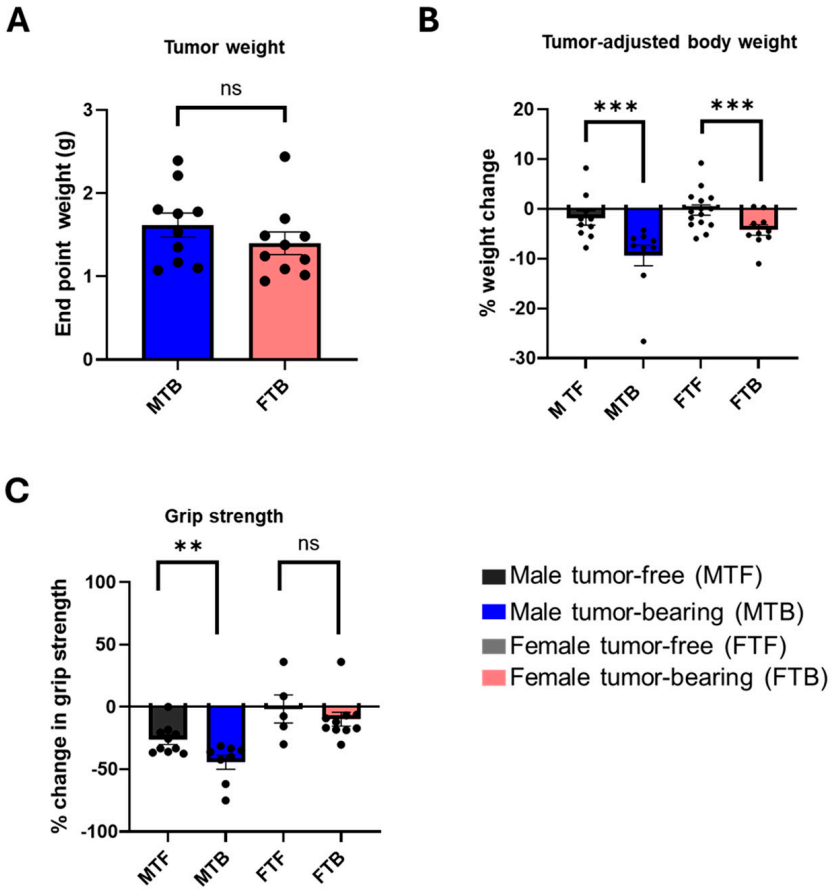


Figure 1. Orthotopic implantation of KPCL-4 pancreatic cancer cells causes loss of body weight and muscle function in C57BL/6J mice. KPCL-4 cells were orthotopically injected into the pancreas of C57BL/6J mice and compared to age and sex-matched tumor-free (TF) mice. (**A**) Endpoint tumor weights after 21 days of tumor implantation for male (MTB) and female tumor-bearing (FTB) mice. (**B**) Percent change in tumor-adjusted body weight of male tumor-free (MTF), MTB, female tumor-free (FTF) and FTB mice at endpoint. (**C**) Percent change in grip strength of MTF, MTB (n = 8), FT (n = 5) F and FTB mice at endpoint. Data represented as mean ± SEM, n = 10/group (unless otherwise stated), ** $p < 0.01$, *** $p < 0.001$.

3.2. KPCL-4 Tumor Induces Hallmarks of Cachexia in a Sex-Specific Manner

We assessed the endpoint weight of skeletal muscles prone to inflammation-induced wasting, such as the gastrocnemius, quadriceps, and tibialis anterior [26]. Aligning with the trend in loss of grip strength (Figure 1C), MTB mice exhibited a significant reduction in the absolute mass of the gastrocnemius, quadricep and tibialis anterior muscles, with mean changes of −18.37%, −22.15% and −31.37%, respectively, relative to MTF mice, whereas FTB mice maintained their skeletal muscle mass (Figure 2A–C). Further, we measured the visceral fat mass (gonadal adipose tissue) in mice across all experimental groups and observed a reduction in MTB and FTB mice relative to their respective TF controls, with MTB mice displaying a more severe fat loss (>50%) as compared to mice of the FTB group (>30%) (Figure 2D). Additionally, while MTB mice demonstrated a 1.29-fold and 3-fold increase in the liver and spleen mass respectively, FTB mice presented a 2.5-fold increase in

the spleen mass without a significant change in the liver, indicating sex-based differences in the severity of cachexia-induced inflammation in these organs (Figure 2E,F).

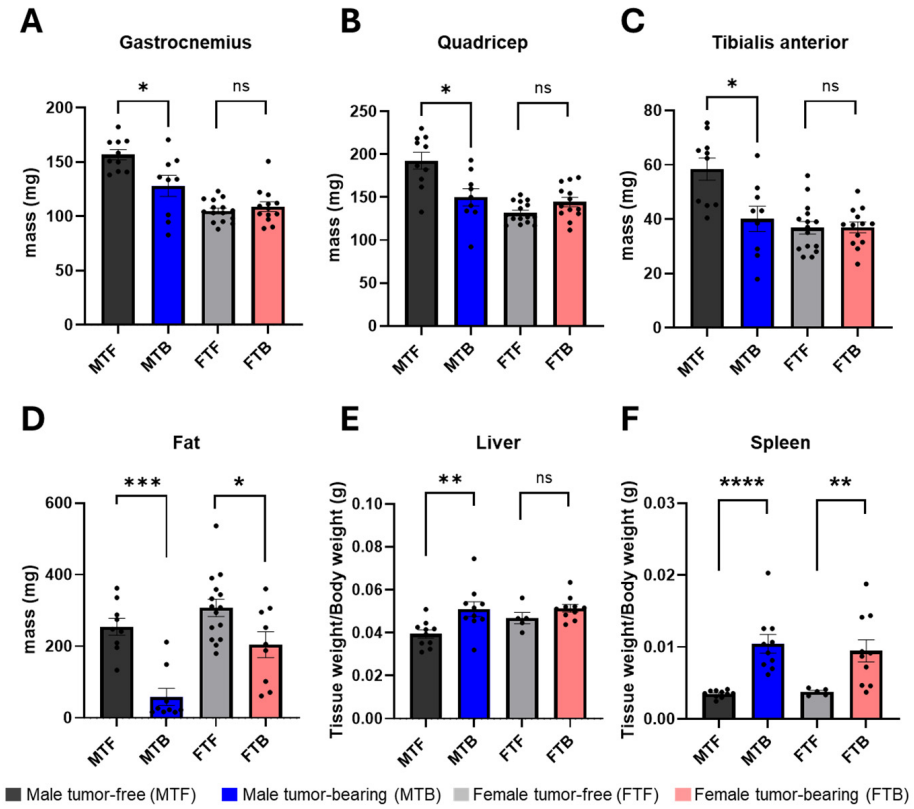


Figure 2. KPCL-4 orthotopic tumor model elicits hallmarks of cachexia, with a strong bias towards males. Several tissues, including skeletal muscles, fat, liver and spleen were harvested from mice at endpoint to assess terminal characteristics of cachexia. Skeletal muscle mass for (**A**) gastrocnemius, (**B**) quadricep and (**C**) tibialis anterior, as recorded after dissection from male tumor-free (MTF, $n = 10$), male tumor-bearing (MTB, $n = 10$), female tumor-free (FTF, $n = 15$) and female tumor-bearing (FTB, $n = 14$) mice at endpoint. Mass of (**D**) visceral fat (gonadal adipose tissue) isolated from MTF ($n = 10$), MTB ($n = 10$), FTF ($n = 15$) and FTB ($n = 14$) mice at endpoint. (**E**) Liver and (**F**) spleen mass as recorded after harvest from MTF ($n = 10$), MTB ($n = 10$), FTF ($n = 5$) and FTB ($n = 10$) mice at endpoint. Data represented as mean ± SEM, * $p < 0.05$, ** $p < 0.01$, *** $p < 0.001$, **** $p < 0.0001$.

3.3. KPCL-4 Pancreatic Cancer Cells Induce Skeletal Muscle Atrophy in Male Mice and Activate the Ubiquitin-Proteasome System

To further confirm that the KPCL-4 tumor induces skeletal muscle atrophy, cryopreserved gastrocnemius muscle cross-sections obtained from MTB, FTB, MTF and FTF mice were stained with Hematoxylin and Eosin (H&E) and Laminin-2. H&E staining revealed a shift in muscle morphology, with MTB and FTB mice demonstrating atrophic features such as shrunken, angular fibers and increased interstitial spaces as opposed to MTF and FTF mice with densely packed polygonal fibers (Figure 3A). Laminin-2 stained muscle cross-sections were subject to muscle fiber cross-sectional area (CSA) quantification using a semi-automated approach (Figure 3B). We analyzed the distribution of myofiber area between MTB and FTB mice relative to the corresponding tumor-free (MTF, FTF) controls since this approach offers valuable insights about complex, non-uniform changes in muscle morphology upon damage, hypertrophy and disease, which can be often overlooked by individual mean values [23]. KPCL-4 tumors induced a shift in the myofiber size distribution towards smaller CSA in both MTB and FTB compared to MTF or FTF mice, respectively ($p < 0.0001$) (Figure 3C–E). This observation was further validated by a Vargha-Delaney

A statistic of a = 0.42 in males and a = 0.35 in females, implying that the myofiber CSA in MTB and FTB mice is stochastically less than their TF counterparts, and confirming the onset of skeletal muscle atrophy in both males and females despite conserved muscle mass in the latter (Figure 2A–C).

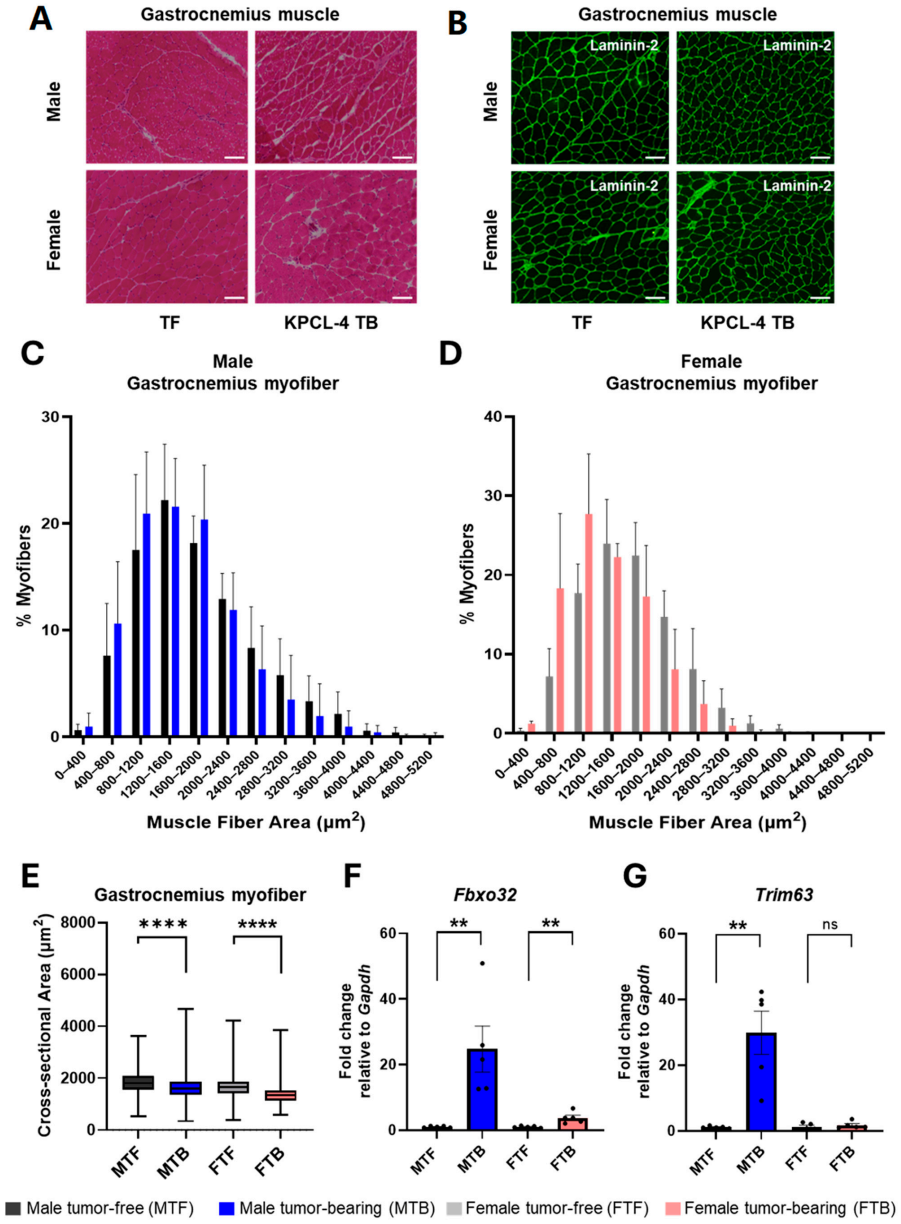


Figure 3. KPCL-4 tumor induces skeletal muscle atrophy and activates E3 ligases in skeletal muscle. Skeletal muscles were assessed for hallmarks of atrophy. Representative 20× objective images of gastrocnemius muscle cryosections from male tumor-free (MTF), male tumor-bearing (MTB), female tumor-free (FTF) and female tumor-bearing (FTB) mice stained for (**A**) Hematoxylin and Eosin, and (**B**) Laminin-2 (Scale bar = 100 µm). (**C**) Frequency plot showing gastrocnemius myofiber cross-sectional area distributions, as % of total mouse myofiber, falling within the designated area ranges for MTF and MTB mice (mean ± SD). (**D**) Frequency plot showing gastrocnemius myofiber cross sectional area distributions, as % of total mouse myofiber, falling within the designated area ranges for FTF and FTB mice (mean ± SD). (**E**) Box and whisker plot of gastrocnemius myofiber cross-sectional area of MTF, MTB, FTF, and FTB mice (mean ± quartiles). (**F**) mRNA expression levels of *Fbxo32* in MTF, MTB, FTF and FTB mice in quadricep muscle, as quantified by RT-qPCR (mean ± SEM). (**G**) mRNA expression levels of *Trim63* in MTF, MTB, FTF and FTB mice in quadricep muscle, as quantified by RT-qPCR (mean ± SEM). $n = 5$, ** $p < 0.01$, **** $p < 0.0001$.

Given the observed loss of skeletal muscle mass and function in males (Figures 1C and 2A–C), we measured the gene expression levels of *Fbxo32* (*Atrogin-1*) and *Trim63* (*MuRF1*) in quadricep muscles of MTB, FTB, MTF and FTF mice. Consistent with the higher severity of skeletal muscle mass loss in males, expression levels of *Fbxo32* and *Trim63* were significantly upregulated in MTB mice relative to the MTF group whereas the FTB mice either experienced comparatively less increase or no significant difference in the mRNA expression of the E3 ligases as compared to their FTF controls (Figure 3F,G).

3.4. KPCL-4 Orthotopic Model Can Be Used as a Tool to Investigate the Immunological Landscape in Cachexia

To investigate the immune landscape in pancreatic cancer cachexia, we designed a high-dimensional spectral flow cytometry panel (Supplementary Figure S2) to holistically stain for systemic (spleen) and tumor-infiltrating innate and adaptive immune populations in MTB and FTB mice at endpoint (n = 10). Within the pancreatic TME of both sexes, we identified 9 distinct clusters of tumor-infiltrating immune cells, including natural killer (NK) cells, M1 and M2 macrophages, conventional dendritic cells (cDC), granulocytic and monocytic myeloid derived suppressor cells (g-MDSCs and m-MDSC), B cells, CD4+ T cells and CD8+ T cells (Figure 4A, Supplementary Figure S2). While quantification of the relative abundance of each immune population as a percentage of CD45+ cells did not reveal any significant differences between male and female tumor-bearing mice, g-MDSCs were notably predominant in both groups (Figure 4B). Additionally, our panel specifically identified distinct phenotypic states of CD4+ and CD8+ T cells such as effector, naïve and memory T cells (Figure 4C). Further, utilizing a SIY-specific fluorescent MHC I tetramer, we quantified the total abundance of SIY-antigen-specific CD8+ T cells (Figure 5A) as well as the abundance of its memory (Figure 5B,C) and exhausted phenotypes (Figure 5D–F) within the pancreatic TME of MTB and FTB mice, but did not find any sex-based differences. Contrastingly, the systemic immune landscape in the spleen revealed interesting sex-based differences, particularly within the T cell compartment. While the global distribution of the broad classes of immune cells including NK cells, NKT cells, M1 and M2 macrophages, cDC, g-MDSC and m-MDSC, B cells, CD4+ and CD8+ T cells were comparable between sexes (Supplementary Figure S3A), FTB mice exhibited a significant increase in the relative abundance of CD8+ central memory T cells compared to MTB mice (Supplementary Figure S3B). Analysis of the SIY-antigen-specific CD8+ T cell populations in the spleen showed that despite similar numbers of total SIY+ CD8+ T cells in MTB and FTB mice, FTB mice demonstrated higher numbers of SIY+ CD8+ effector memory and stem-like effector cells relative to MTB mice without significant differences in the central memory, stem-like or exhausted phenotypes (Supplementary Figure S3C–H). These findings indicate a divergence between local and systemic immunity in tumor-bearing mice, highlighting the importance of characterizing systemic cytokines and inflammatory mediators, which may act as critical drivers of sexual dimorphism in cachexia presentation in the KPCL-4 tumor model.

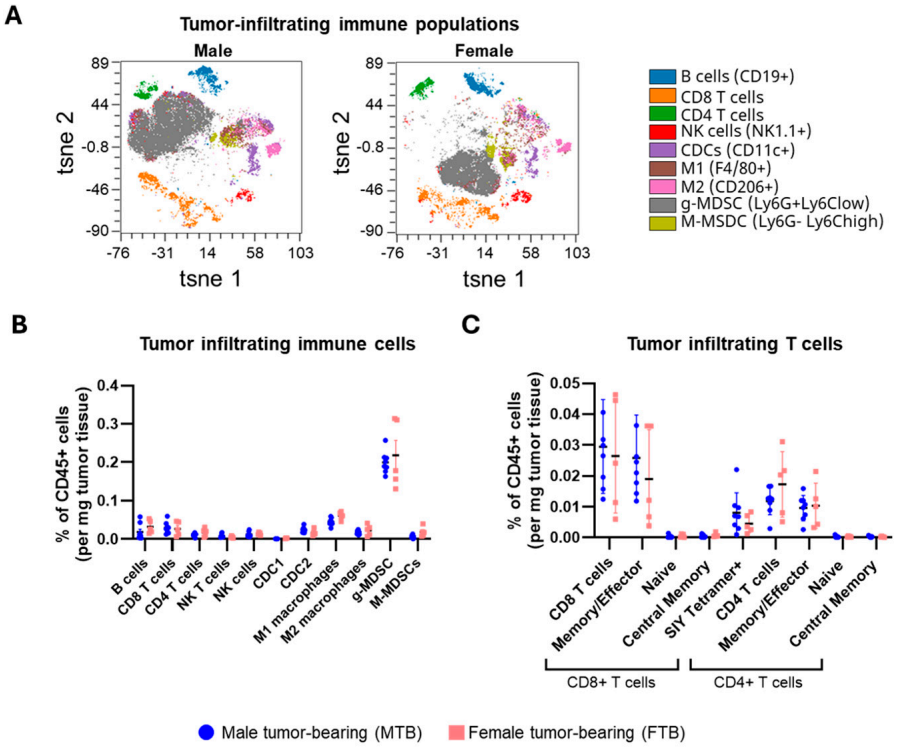


Figure 4. Intra-tumoral immune landscape in KPCL-4 tumor-bearing mice. Tumor-infiltrating immune populations were isolated and stained for spectral flow cytometry. (**A**) Representative tSNE plots showing tumor-infiltrating immune populations in male (MTB) and female (FTB) KPCL-4 tumor-bearing mice. Relative abundance of (**B**) tumor-infiltrating immune populations and (**C**) tumor-infiltrating T cell subpopulations as a percentage of CD45+ hematopoietic cells, normalized to the tumor weight in MTB (n = 8) and FTB (n = 5) mice. Data presented as mean ± SD.

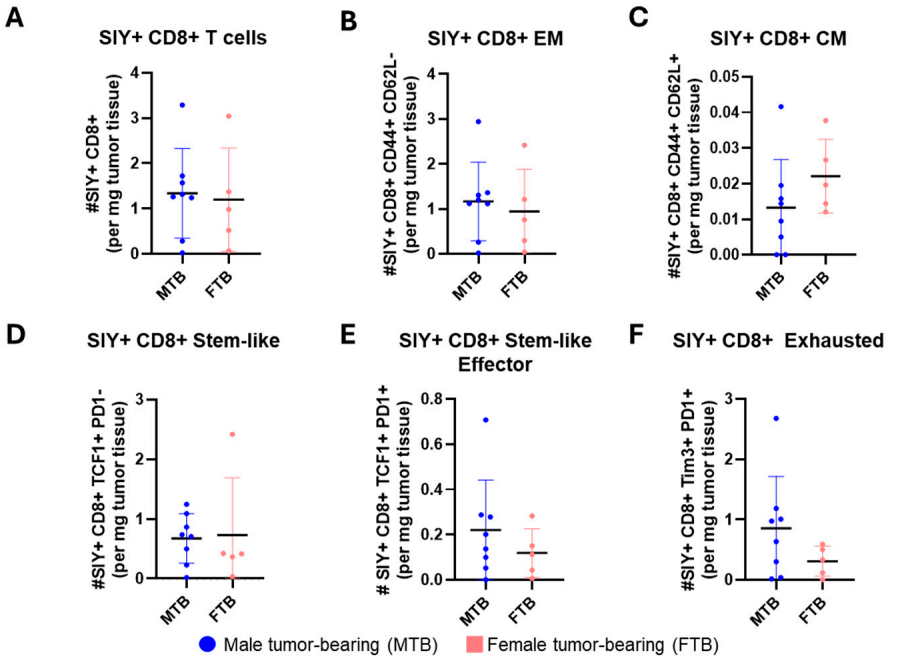


Figure 5. The KPCL-4 tumor model allows investigation of SIY-antigen specific T cell phenotypes. Number (#) of SIY$^+$ CD8$^+$ (**A**) T cells, (**B**) effector/memory (EM; CD44$^+$ CD62L$^-$), (**C**) central memory (CM; CD44$^+$ CD62L$^+$), (**D**) stem-like (Tim3$^-$ TCF1$^+$ PD1$^-$), (**E**) stem-like effector (Tim3$^-$ TCF1$^+$ PD1$^+$) and (**F**) exhausted (Tim3$^+$ PD1$^+$) T cells, normalized to the tumor weight in MTB (n = 8) and FTB (n = 5) mice. Data presented as mean ± SD.

3.5. The KPCL-4 PDAC Model Elicits Sex Bias in Circulating Inflammatory Markers

As we did not find sex bias in the relative abundance of various intra-tumoral immune populations, it is plausible that the inflammatory factors secreted by the tumor and tumor-associated immune populations are more potent drivers of differential skeletal muscle wasting in male and female KPCL-4 tumor-bearing mice. We quantified the terminal plasma cytokine profiles in MTB (severely cachectic) and FTB mice, along with the respective tumor-free controls (MTF and FTF), using a 32-cytokine Bioplex panel. We observed higher circulating levels of proinflammatory cytokines including IL-6, LIF and G-CSF in MTB and FTB mice relative to MTF and FTF controls respectively, without any statistically significant differences between MTB and FTB groups. (Figure 6A–C). However, TNF-α upregulation was particularly striking in males. MTB mice exhibited a 1.8-fold increase in plasma TNF-α concentration relative to MTF controls and 1.4-fold higher levels than FTB mice, suggesting a prominent role of this cytokine in the sex-specific presentation of cachexia (Figure 6D). We also observed a bias in inflammatory cytokines such as RANTES (CXCL5), LIX (CCL5) and IL-15 towards males, whereby MTB mice showed a more than 2-fold downregulation in comparison to MTF controls (Figures 6E,F and 7A) whereas females did not show any differences. Few proinflammatory cytokines and chemokines such as IL1-β, Eotaxin, IP-10, MCP-1, MIP1-α and VEGF were differentially upregulated in either MTB or FTB mice relative to the sex-matched TF controls, but no sex-based differences were noted in tumor-bearing mice (Supplementary Figure S4). Further, while MTB mice did not demonstrate any significant change in cytokines associated with T cell activity including IL-2, IFN-γ, IL-5, MIP1-β and MIG, these cytokines presented a more than 3-fold increase in FTB mice (Figure 7B–F), suggesting the potential involvement of these cytokines in counteracting cachexia-associated inflammatory pathways in females without influencing tumor growth. Therefore, the sex bias in cachexia presentation in the KPCL-4 tumor-bearing model likely stems from differences in immune cell activity governing inflammatory mediators, opening avenues for strategically optimizing the male and female tumor-bearing animals for diverse preclinical applications.

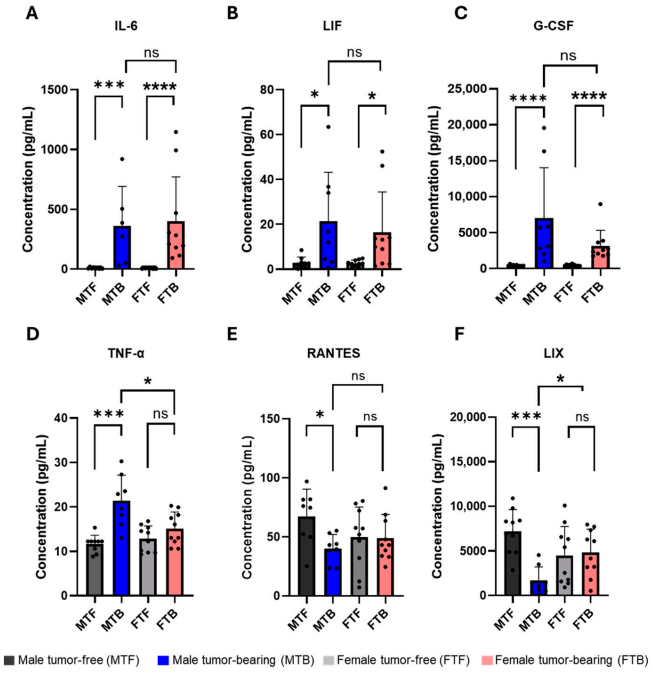


Figure 6. KPCL-4 tumors result in upregulation of inflammatory cytokines in the plasma of tumor-bearing mice. Terminal circulating plasma cytokine concentrations of (**A**) IL-6, (**B**) LIF, (**C**) G-CSF, (**D**) TNF-α, (**E**) RANTES, and (**F**) LIX in male tumor-free (MTF, $n = 10$), male tumor-bearing (MTB, $n = 8$), female tumor-free (FTF, $n = 10$) and female tumor-bearing (FTB, $n = 10$) mice. Data represented as mean ± SD, * $p < 0.05$, *** $p < 0.001$, **** $p < 0.0001$.

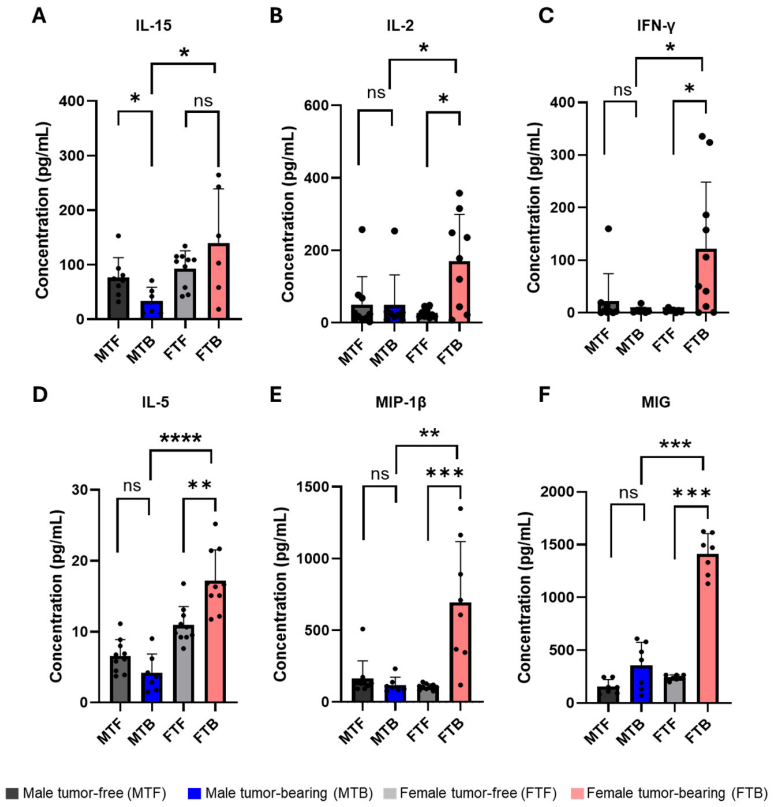


Figure 7. Female KPCL-4 tumor-bearing mice have elevated T cell-associated cytokines in circulation. Terminal circulating plasma cytokine concentrations of (**A**) IL-15, (**B**) IL-2, (**C**) IFN-γ, (**D**) IL-5, (**E**) MIP-1β and (**F**) MIG in male tumor-free (MTF, $n = 10$), male tumor-bearing (MTB, $n = 8$), female tumor-free (FTF, $n = 10$) and female tumor-bearing (FTB, $n = 10$) mice. Data represented as mean ± SD, * $p < 0.05$, ** $p < 0.01$, *** $p < 0.001$, **** $p < 0.0001$.

4. Discussion

Cachexia is a predominant contributor to the mortality and morbidity of pancreatic cancer. Apart from reducing the quality of life of affected individuals, the presence of cachexia reduces the effectiveness of various chemotherapeutic and immunotherapeutic regimes [2]. Despite substantial advancements in the mechanistic understanding of the syndrome and several established preclinical models, the additive effects of cancer and its therapeutic interventions on the mechanisms governing cachexia progression remain poorly understood, necessitating further investigation in novel preclinical models [27]. In this report, we have characterized a novel pancreatic cancer cachexia model in the immunocompetent C57BL/6J mice by utilizing the SIY-antigen expressing KPC-derived pancreatic cancer cell line named KPCL-4 [20]. We conclude that this murine model reflects clinically relevant hallmarks of cachexia and holds immense potential to be employed as a valuable tool for investigating the crosstalk between pancreatic cancer cachexia and immunoregulatory pathways.

From patients to mice models, research has hinted towards the heterogeneity of cancer-associated cachexia between biological sex during its development in pancreatic cancer. Concurrent with clinical presentation, in our study, FTB mice exhibited relatively preserved muscle mass despite other hallmarks of cachexia including splenomegaly, loss of visceral fat and elevated expression of *Fbxo32* (Figures 2 and 3F). This is consistent with other investigations in the KPC model of pancreatic cancer as well as the C26 colon carcinoma model, and is especially interesting since the tumor burden was not significantly different in males or females, indicating an inherent sexual basis of skeletal muscle preservation in

females [7,8]. Hormonal differences and mitochondria can both play a role in inducing such sex-specific differences in different cell types which could affect muscle health as well as responses towards adipose tissue wasting [9,28,29]. In fact, the reproductive hormone activin has been found to be a sex-specific driver of muscle wasting in male KPC mice with autochthonous pancreatic ductal adenocarcinoma (PDAC) [7]. However, concurrent with recent investigations into the phases of metabolic reprogramming in PDAC which revealed that fat loss often precedes muscle wasting in the development of cachexia, another possibility is that females have a slower onset of cachexia as opposed to males whereby their fat loss has become apparent in the 21-day timeline of our study and muscle wasting is yet to happen [30]. Additionally, the fact that FTB mice display a relatively preserved muscle mass despite an increase in *Fbxo32* and smaller muscle cross-sectional area (Figure 3), supports the emerging shift in the current paradigm of cachexia evaluation from simplistic body weight and muscle mass assessments to a more holistic approach. Indeed, the absence of longitudinal body composition measurements of MTB and FTB mice in our study limits our ability to definitively map sex-based differences in disease trajectory in the KPCL-4 tumor model, necessitating non-invasive longitudinal assessments of muscle and fat mass in future investigations to confirm whether the KPCL-4 tumor model reflects a true sex bias in cachexia presentation or merely a temporal delay in disease progression in females.

While several studies underscore the involvement of muscle resident immune cells such as macrophages, T cells and neutrophils in regulating processes underlying skeletal muscle homeostasis, the impact of tumor-induced immune responses on these mechanisms during cachexia remains largely unexplored [31–33]. Given the role of immune cells in regulating repair, remodeling and overall plasticity of skeletal muscles, it is plausible that immunotherapeutic interventions could impact these pathways, consequently disrupting muscle homeostasis. Recent investigations have revealed an inverse association between cachexia and response to immunotherapies in several cancers, especially in non-small cell lung cancer (NSCLC) [17,18]. This holds immense implications in PDAC, where more than 80% of patients eventually develop cachexia and immunotherapy is yet to make a notable difference in clinical outcomes [5,16]. In order to optimize immunotherapeutic approaches and develop novel interventions in PDAC, further mechanistic studies are required in effective preclinical models. In this report, we quantified the relative abundance of the broad classes of innate and adaptive immune populations as well as identified distinct subpopulations of tumor-infiltrating T cells in MTB and FTB cachectic mice but did not observe any apparent sex bias in the predominance of the assessed immune populations within the pancreatic TME (Figure 4). Notably, KPCL-4 is a female-derived cell line and could possibly have a proinflammatory, immunogenic reaction when implanted in a male recipient, accounting for the more severe cachectic phenotype in the latter. However, since we did not observe any statistically significant differences in the abundance of tumor-infiltrating immune populations (Figure 4B,C), SIY tetramer+ CD8 T (Figure 5) cells as well as the tumor weight (Figure 1A), we believe the mechanisms underlying differential cachexia presentation in male and female C57BL/6 mice are beyond a direct immunogenic reaction to the cell line. Importantly, the ability to investigate SIY-antigen-specific T cell phenotypes in KPCL-4 tumor-bearing mice opens novel avenues for studying immune impairment in cachexia, shedding light on the crosstalk between cachexia and anti-tumor immunity. Although further studies directly validating effector T cell function (e.g., cytotoxicity or cytokine production ex vivo) in the KPCL-4 model are necessary to characterize antigen specific immune function, the scope of identifying and tracking SIY-antigen specific T cells with distinct phenotypic profiles (effector, memory and exhausted) in KPCL-4 tumor-bearing mice expands the clinical relevance of this model, making it a versatile tool for further preclinical studies. While the primary objective of this study was the development

and characterization of a novel, immunocompetent pancreatic cancer cachexia model, it sets the stage for future investigations aimed at optimizing immunotherapies in the presence of cachexia.

The onset of cancer cachexia is primarily driven by systemic inflammation orchestrated by tumor-secreted factors, which act in concert with immune cells and peripheral tissues to elicit sustained local inflammation in different organs in cachectic individuals. A recent study illustrated that local tissue inflammation during cachexia triggers nuclear factor κB (NF-κB) dependent macrophage accumulation within skeletal muscles, leading to muscle atrophy via the inhibition of muscle regeneration [34]. Thus, it is possible that tumor-secreted factors in the circulation induce changes in the local immune milieu within various target organs, and such local inflammation in specific niches is a more potent driver of cachexia. Consequently, profiling the tumor secretome in the plasma offers a non-invasive approach to understanding the inflammatory landscape and identifying potential biomarkers for the early detection of cachexia in patients, aiding early-stage disease management. In this study, we assessed the endpoint circulating concentrations of several inflammatory cytokines in the plasma of mice across all experimental groups. Notably, TNF-α was specifically upregulated in MTB mice (Figure 6D), representing a systemic profile that is often associated with a cachectic phenotype in murine models of cachexia. Indeed, TNF-α has been shown to drive skeletal muscle wasting via the activation of the ubiquitin-proteasome system [35], which aligns with the increase in *Fbxo32* and *Trim63* in our model (Figure 3F,G). Additionally, we observed significantly lower levels of IL-15 in MTB mice relative to MTF and FTB mice (Figure 7A). While IL-15 has been reported to antagonize TNF-α-mediated muscle loss suggesting the involvement of TNF-α in driving cachexia in this model, it is important to note that these cytokine profiles are associative and further mechanistic studies are required to validate these hypotheses [36,37]. Further, we report significant downregulation of RANTES (CCL5) in MTB mice and upregulation of IL-15, IL-2, IFN-γ and IL-5, MIP1-β and MIG in FTB mice relative to males (Figures 6 and 7). These cytokines are closely associated with T cell activation, proliferation and infiltration in several cancers [38–41]. In combination with the observed increase in CD8+ central memory, SIY+ CD8+ effector memory and SIY+ CD8+ stem-like effector T cells in the spleens of FTB mice (Supplementary Figure S3), these results suggest the potential involvement of T cell-associated responses in mitigating cachexia-associated inflammatory pathways in FTB mice. However, further investigation of predominant immune cell phenotypes and downstream signaling pathways in skeletal muscles and other peripheral tissues is critical to establish a direct causal link between these circulating inflammatory markers, immune populations and the observed differences in the cachectic phenotype of MTB and FTB mice. Such a mechanistic understanding of the model will aid in further characterization of the KPCL-4 tumor model as a valuable translational tool for evaluating cytokine and adoptive T cell-based immunotherapies in the context of pancreatic cancer cachexia.

Some important limitations of our work include the utilization of a single cell line (KPCL-4) in this PDAC cachexia model. While the utilization of this cell line allowed a granular analysis of sex-specific differences and the immune landscape in PDAC-associated cachexia, we recognize the need of validating these findings across additional cell lines in future investigations to ensure broad applicability of the model. Another limitation of this study includes the use of 8–10-week-old mice which corresponds to 15–20-year-old humans [42,43]. Although the use of young mice to model cancer cachexia is common, the average age of PDAC patients is 50–70 years which raises questions about whether the KPCL-4 model of pancreatic cancer cachexia truly replicates human disease [44]. Further, prior work suggests that anorexia is a common cachectic parameter in clinics as well as murine models, raising the importance of assessing food consumption of mice across

experimental groups [45,46]. Although we do not observe any significant difference in the average food consumption of males versus females (Supplementary Figure S1), our data is limited by the fact that it is calculated as a cage average rather than on a per-mouse basis, which could have introduced bias in our reported data. Lastly, the lack of statistical significance in intra-tumoral SIY-antigen-specific T cell abundance between male and female tumor-bearing mice should be interpreted with caution, as our analysis was limited to a small cohort (n = 5), underscoring the need for a more in-depth study of immune cell abundance and activity before employing this model for the preclinical evaluation of immune-based therapies.

5. Conclusions

We have characterized a novel murine model of pancreatic cancer cachexia that faithfully captures clinical hallmarks of cachexia including unintentional weight loss, a reduction in skeletal muscle mass and functionality, the upregulation of ubiquitin ligases in skeletal muscles, loss of visceral fat, and inflammation in the liver and spleen. Interestingly, the inherent sexual bias towards the manifestation of the cachectic phenotype, as seen in human PDAC patients and other murine models, was conserved in KPCL-4 tumor-bearing mice. Finally, this study yields a robust, immunocompetent murine model of pancreatic cancer cachexia that can be employed for future investigations to test hypotheses regarding sex-specific differences in immunotherapy response and the potential of cachexia to serve as a prognostic factor for predicting immunotherapy outcomes in PDAC.

Supplementary Materials: The following supporting information can be downloaded at https://www.mdpi.com/article/10.3390/cancers18040587/s1, Supplemental Figures: Figure S1: Average food consumption per cage. Figure S2: Gating strategy for various immune cells analyzed by spectral flow cytometry analysis of tumor-infiltrating lymphocytes. Figure S3: Immune landscape in the spleen of KPCL-4 tumor-bearing mice. Figure S4: Plasma cytokine concentrations.

Author Contributions: A.D., D.M., L.D., J.W., M.S., H.L. and J.L. performed experiments. A.G. (Abigail Guenther), M.K., J.V., B.R., S.K.K., J.T., K.K. and A.A. assisted with experiments. A.D., D.M., S.C. and T.A.M. analyzed data. A.D., D.M., M.A.P., C.C.C. and T.A.M. conceived and designed the project. J.A.R.-F., S.C., A.G. (Andrew Gunderson), M.A.P. and C.C.C. provided valuable insight and instruction. A.D., D.M. and T.A.M. wrote the manuscript. All authors have read and agreed to the published version of the manuscript.

Funding: This project was supported by the OSU Comprehensive Cancer Center (OSUCCC-P30CA016058), Pelotonia Institute for Immuno-Oncology (PIIO), which is funded by the Pelotonia community and the OSUCCC. This study was further supported by National Cancer Institute grants R01 CA273924 and the NIH Tetramer Core Facility (NIH Contract 75N93020D00005 and RRID:SCR_026557) provided the SIY tetramers utilized in these studies. The research was supported by the Pelotonia Graduate Fellowship Program and OSU Presidential Fellowship.

Institutional Review Board Statement: All animal protocols were approved by the Institutional Animal Care and Use Committee (IACUC) at The Ohio State University (2009A0178-R5, approved 22 May 2024) and mice were treated in accordance with institutional guidelines for animal care. The Ohio State University Laboratory Animal Shared Resource is an Association for Assessment and Accreditation of Laboratory Animal Care International accredited program that follows Public Health Service policy and guidelines. All other experiments were completed under the research protocols (2014R00000086; 2013R00000056) approved by the Ohio State University Institutional Biosafety Committee.

Data Availability Statement: The data that support the findings of this study are available from the corresponding author upon reasonable request.

Conflicts of Interest: The authors declare no conflicts of interest.

References

1. Baracos, V.E.; Martin, L.; Korc, M.; Guttridge, D.C.; Fearon, K.C.H. Cancer-associated cachexia. *Nat. Rev. Dis. Primers* **2018**, *4*, 17105. [CrossRef] [PubMed]
2. Fearon, K.; Strasser, F.; Anker, S.D.; Bosaeus, I.; Bruera, E.; Fainsinger, R.L.; Jatoi, A.; Loprinzi, C.; MacDonald, N.; Mantovani, G.; et al. Definition and classification of cancer cachexia: An international consensus. *Lancet Oncol.* **2011**, *12*, 489–495. [CrossRef] [PubMed]
3. Palesty, J.A.; Dudrick, S.J. What we have learned about cachexia in gastrointestinal cancer. *Dig. Dis.* **2003**, *21*, 198–213. [CrossRef] [PubMed]
4. Felix, K.; Fakelman, F.; Hartmann, D.; Giese, N.A.; Gaida, M.M.; Schnolzer, M.; Flad, T.; Buchler, M.W.; Werner, J. Identification of serum proteins involved in pancreatic cancer cachexia. *Life Sci.* **2011**, *88*, 218–225. [CrossRef] [PubMed]
5. Poulia, K.A.; Sarantis, P.; Antoniadou, D.; Koustas, E.; Papadimitropoulou, A.; Papavassiliou, A.G.; Karamouzis, M.V. Pancreatic Cancer and Cachexia-Metabolic Mechanisms and Novel Insights. *Nutrients* **2020**, *12*, 1543. [CrossRef] [PubMed] [PubMed Central]
6. Stephens, N.A.; Gray, C.; MacDonald, A.J.; Tan, B.H.; Gallagher, I.J.; Skipworth, R.J.; Ross, J.A.; Fearon, K.C.; Greig, C.A. Sexual dimorphism modulates the impact of cancer cachexia on lower limb muscle mass and function. *Clin. Nutr.* **2012**, *31*, 499–505. [CrossRef] [PubMed]
7. Zhong, X.; Narasimhan, A.; Silverman, L.M.; Young, A.R.; Shahda, S.; Liu, S.; Wan, J.; Liu, Y.; Koniaris, L.G.; Zimmers, T.A. Sex specificity of pancreatic cancer cachexia phenotypes, mechanisms, and treatment in mice and humans: Role of Activin. *J. Cachexia Sarcopenia Muscle* **2022**, *13*, 2146–2161. [CrossRef] [PubMed] [PubMed Central]
8. Cabrera, A.R.; Deaver, J.W.; Lim, S.; Morena da Silva, F.; Schrems, E.R.; Saling, L.W.; Tsitkanou, S.; Rosa-Caldwell, M.E.; Wiggs, M.P.; Washington, T.A.; et al. Females display relatively preserved muscle quality compared with males during the onset and early stages of C26-induced cancer cachexia. *J. Appl. Physiol.* **2023**, *135*, 655–672. [CrossRef] [PubMed] [PubMed Central]
9. White, J.P.; Puppa, M.J.; Sato, S.; Gao, S.; Price, R.L.; Baynes, J.W.; Kostek, M.C.; Matesic, L.E.; Carson, J.A. IL-6 regulation on skeletal muscle mitochondrial remodeling during cancer cachexia in the ApcMin/+ mouse. *Skelet. Muscle* **2012**, *2*, 14. [CrossRef] [PubMed] [PubMed Central]
10. Liu, M.; Ren, Y.; Zhou, Z.; Yang, J.; Shi, X.; Cai, Y.; Arreola, A.X.; Luo, W.; Fung, K.M.; Xu, C.; et al. The crosstalk between macrophages and cancer cells potentiates pancreatic cancer cachexia. *Cancer Cell* **2024**, *42*, 885–903.e4. [CrossRef] [PubMed] [PubMed Central]
11. Flint, T.R.; Janowitz, T.; Connell, C.M.; Roberts, E.W.; Denton, A.E.; Coll, A.P.; Jodrell, D.I.; Fearon, D.T. Tumor-Induced IL-6 Reprograms Host Metabolism to Suppress Anti-tumor Immunity. *Cell Metab.* **2016**, *24*, 672–684. [CrossRef] [PubMed] [PubMed Central]
12. Chang, C.H.; Qiu, J.; O'Sullivan, D.; Buck, M.D.; Noguchi, T.; Curtis, J.D.; Chen, Q.; Gindin, M.; Gubin, M.M.; van der Windt, G.J.; et al. Metabolic Competition in the Tumor Microenvironment Is a Driver of Cancer Progression. *Cell* **2015**, *162*, 1229–1241. [CrossRef] [PubMed] [PubMed Central]
13. Ho, P.C.; Bihuniak, J.D.; Macintyre, A.N.; Staron, M.; Liu, X.; Amezquita, R.; Tsui, Y.C.; Cui, G.; Micevic, G.; Perales, J.C.; et al. Phosphoenolpyruvate Is a Metabolic Checkpoint of Anti-tumor T Cell Responses. *Cell* **2015**, *162*, 1217–1228. [CrossRef] [PubMed] [PubMed Central]
14. Lahiri, A.; Maji, A.; Potdar, P.D.; Singh, N.; Parikh, P.; Bisht, B.; Mukherjee, A.; Paul, M.K. Lung cancer immunotherapy: Progress, pitfalls, and promises. *Mol. Cancer* **2023**, *22*, 40. [CrossRef] [PubMed] [PubMed Central]
15. Liu, C.; Yang, M.; Zhang, D.; Chen, M.; Zhu, D. Clinical cancer immunotherapy: Current progress and prospects. *Front. Immunol.* **2022**, *13*, 961805. [CrossRef] [PubMed] [PubMed Central]
16. Principe, D.R.; Korc, M.; Kamath, S.D.; Munshi, H.G.; Rana, A. Trials and tribulations of pancreatic cancer immunotherapy. *Cancer Lett.* **2021**, *504*, 1–14. [CrossRef] [PubMed] [PubMed Central]
17. Miyawaki, T.; Naito, T.; Kodama, A.; Nishioka, N.; Miyawaki, E.; Mamesaya, N.; Kawamura, T.; Kobayashi, H.; Omori, S.; Wakuda, K.; et al. Desensitizing Effect of Cancer Cachexia on Immune Checkpoint Inhibitors in Patients With Advanced NSCLC. *JTO Clin. Res. Rep.* **2020**, *1*, 100020. [CrossRef] [PubMed] [PubMed Central]
18. Matsuo, N.; Azuma, K.; Murotani, K.; Murata, D.; Matama, G.; Kawahara, A.; Kojima, T.; Tokito, T.; Hoshino, T. Prognostic effect of cachexia in patients with non-small cell lung cancer receiving immune checkpoint inhibitors. *Thorac. Cancer* **2023**, *14*, 1362–1367. [CrossRef] [PubMed] [PubMed Central]
19. Castillo, A.M.M.; Vu, T.T.; Liva, S.G.; Chen, M.; Xie, Z.; Thomas, J.; Remaily, B.; Guo, Y.; Subrayan, U.L.; Costa, T.; et al. Murine cancer cachexia models replicate elevated catabolic pembrolizumab clearance in humans. *JCSM Rapid Commun.* **2021**, *4*, 232–244. [CrossRef] [PubMed] [PubMed Central]
20. Medler, T.R.; Kramer, G.; Bambina, S.; Gunderson, A.J.; Alice, A.; Blair, T.; Zebertavage, L.; Duhen, T.; Duhen, R.; Young, K.; et al. Tumor resident memory CD8 T cells and concomitant tumor immunity develop independently of CD4 help. *Sci. Rep.* **2023**, *13*, 6277. [CrossRef] [PubMed] [PubMed Central]

21. Sun, M.; Choi, E.Y.; Magee, D.J.; Stets, C.W.; During, M.J.; Lin, E.J. Metabolic Effects of Social Isolation in Adult C57BL/6 Mice. *Int. Sch. Res. Not.* **2014**, *2014*, 690950. [CrossRef] [PubMed] [PubMed Central]
22. Zhao, X.; Li, F.; Cheng, C.; Bi, M.; Li, J.; Cong, J.; Wang, X. Social isolation promotes tumor immune evasion via beta2-adrenergic receptor. *Brain Behav. Immun.* **2025**, *123*, 607–618. [CrossRef] [PubMed]
23. Gilda, J.E.; Ko, J.H.; Elfassy, A.Y.; Tropp, N.; Parnis, A.; Ayalon, B.; Jhe, W.; Cohen, S. A semiautomated measurement of muscle fiber size using the Imaris software. *Am. J. Physiol. Cell Physiol.* **2021**, *321*, C615–C631. [CrossRef] [PubMed]
24. Liva, S.G.; Tseng, Y.C.; Dauki, A.M.; Sovic, M.G.; Vu, T.; Henderson, S.E.; Kuo, Y.C.; Benedict, J.A.; Zhang, X.; Remaily, B.C.; et al. Overcoming resistance to anabolic SARM therapy in experimental cancer cachexia with an HDAC inhibitor. *EMBO Mol. Med.* **2020**, *12*, e9910. [CrossRef] [PubMed] [PubMed Central]
25. Nakao, R.; Okauchi, H.; Hashimoto, C.; Wada, N.; Oishi, K. Determination of reference genes that are independent of feeding rhythms for circadian studies of mouse metabolic tissues. *Mol. Genet. Metab.* **2017**, *121*, 190–197. [CrossRef] [PubMed]
26. Braun, T.P.; Zhu, X.; Szumowski, M.; Scott, G.D.; Grossberg, A.J.; Levasseur, P.R.; Graham, K.; Khan, S.; Damaraju, S.; Colmers, W.F.; et al. Central nervous system inflammation induces muscle atrophy via activation of the hypothalamic-pituitary-adrenal axis. *J. Exp. Med.* **2011**, *208*, 2449–2463. [CrossRef] [PubMed] [PubMed Central]
27. Barreto, R.; Mandili, G.; Witzmann, F.A.; Novelli, F.; Zimmers, T.A.; Bonetto, A. Cancer and Chemotherapy Contribute to Muscle Loss by Activating Common Signaling Pathways. *Front. Physiol.* **2016**, *7*, 472. [CrossRef] [PubMed] [PubMed Central]
28. Demarest, T.G.; McCarthy, M.M. Sex differences in mitochondrial (dys)function: Implications for neuroprotection. *J. Bioenerg. Biomembr.* **2015**, *47*, 173–188. [CrossRef] [PubMed] [PubMed Central]
29. Lim, S.; Deaver, J.W.; Rosa-Caldwell, M.E.; Haynie, W.S.; Morena da Silva, F.; Cabrera, A.R.; Schrems, E.R.; Saling, L.W.; Jansen, L.T.; Dunlap, K.R.; et al. Development of metabolic and contractile alterations in development of cancer cachexia in female tumor-bearing mice. *J. Appl. Physiol.* **2022**, *132*, 58–72. [CrossRef] [PubMed] [PubMed Central]
30. Sah, R.P.; Sharma, A.; Nagpal, S.; Patlolla, S.H.; Sharma, A.; Kandlakunta, H.; Anani, V.; Angom, R.S.; Kamboj, A.K.; Ahmed, N.; et al. Phases of Metabolic and Soft Tissue Changes in Months Preceding a Diagnosis of Pancreatic Ductal Adenocarcinoma. *Gastroenterology* **2019**, *156*, 1742–1752. [CrossRef] [PubMed] [PubMed Central]
31. Pizza, F.X.; Peterson, J.M.; Baas, J.H.; Koh, T.J. Neutrophils contribute to muscle injury and impair its resolution after lengthening contractions in mice. *J. Physiol.* **2005**, *562*, 899–913. [CrossRef] [PubMed] [PubMed Central]
32. Arnold, L.; Henry, A.; Poron, F.; Baba-Amer, Y.; van Rooijen, N.; Plonquet, A.; Gherardi, R.K.; Chazaud, B. Inflammatory monocytes recruited after skeletal muscle injury switch into antiinflammatory macrophages to support myogenesis. *J. Exp. Med.* **2007**, *204*, 1057–1069. [CrossRef] [PubMed] [PubMed Central]
33. Zhang, J.; Xiao, Z.; Qu, C.; Cui, W.; Wang, X.; Du, J. CD8 T cells are involved in skeletal muscle regeneration through facilitating MCP-1 secretion and Gr1(high) macrophage infiltration. *J. Immunol.* **2014**, *193*, 5149–5160. [CrossRef] [PubMed]
34. Pryce, B.R.; Oles, A.; Talbert, E.E.; Romeo, M.J.; Vaena, S.; Sharma, S.; Spadafora, V.; Tolliver, L.; Mahvi, D.A.; Morgan, K.A.; et al. Muscle inflammation is regulated by NF-kappaB from multiple cells to control distinct states of wasting in cancer cachexia. *Cell Rep.* **2024**, *43*, 114925. [CrossRef] [PubMed] [PubMed Central]
35. Patel, H.J.; Patel, B.M. TNF-alpha and cancer cachexia: Molecular insights and clinical implications. *Life Sci.* **2017**, *170*, 56–63. [CrossRef] [PubMed]
36. Carbo, N.; Lopez-Soriano, J.; Costelli, P.; Busquets, S.; Alvarez, B.; Baccino, F.M.; Quinn, L.S.; Lopez-Soriano, F.J.; Argiles, J.M. Interleukin-15 antagonizes muscle protein waste in tumour-bearing rats. *Br. J. Cancer* **2000**, *83*, 526–531. [CrossRef] [PubMed] [PubMed Central]
37. O'Leary, M.F.; Wallace, G.R.; Bennett, A.J.; Tsintzas, K.; Jones, S.W. IL-15 promotes human myogenesis and mitigates the detrimental effects of TNFalpha on myotube development. *Sci. Rep.* **2017**, *7*, 12997. [CrossRef] [PubMed] [PubMed Central]
38. Blomberg, O.S.; Spagnuolo, L.; Garner, H.; Voorwerk, L.; Isaeva, O.I.; van Dyk, E.; Bakker, N.; Chalabi, M.; Klaver, C.; Duijst, M.; et al. IL-5-producing $CD4^+$ T cells and eosinophils cooperate to enhance response to immune checkpoint blockade in breast cancer. *Cancer Cell* **2023**, *41*, 106–123e10. [CrossRef] [PubMed]
39. Kohli, K.; Pillarisetty, V.G.; Kim, T.S. Key chemokines direct migration of immune cells in solid tumors. *Cancer Gene Ther.* **2022**, *29*, 10–21. [CrossRef] [PubMed] [PubMed Central]
40. Zhang, Y.; Guan, X.Y.; Jiang, P. Cytokine and Chemokine Signals of T-Cell Exclusion in Tumors. *Front. Immunol.* **2020**, *11*, 594609. [CrossRef]
41. Pilipow, K.; Roberto, A.; Roederer, M.; Waldmann, T.A.; Mavilio, D.; Lugli, E. IL15 and T-cell Stemness in T-cell-Based Cancer Immunotherapy. *Cancer Res.* **2015**, *75*, 5187–5193. [CrossRef] [PubMed] [PubMed Central]
42. Wang, S.; Lai, X.; Deng, Y.; Song, Y. Correlation between mouse age and human age in anti-tumor research: Significance and method establishment. *Life Sci.* **2020**, *242*, 117242. [CrossRef] [PubMed]
43. Remaily, B.C.; Vu, T.T.; Thomas, J.; Kim, K.; Stanton, C.; Xie, Z.; Granchie, L.; Manna, M.; Gregorevic, P.; Mo, X.; et al. Intramuscular CMT-167 Tumors Produce a Mild Cachexia Phenotype in C57BL/6J Mice. *JCSM Commun.* **2025**, *8*, e117. [CrossRef] [PubMed] [PubMed Central]

44. Siegel, R.L.; Kratzer, T.B.; Giaquinto, A.N.; Sung, H.; Jemal, A. Cancer statistics, 2025. *CA Cancer J. Clin.* **2025**, *75*, 10–45. [CrossRef] [PubMed] [PubMed Central]
45. Dev, R.; Bramati, P.; Guay Marvin Omar, D.; Fellman, B.; Azhar, A.; Tang, M.; Tennison, J.; Becerra, J.; Admane, S.; Dalal, S.; et al. Malnutrition Risk and the Psychological Burden of Anorexia and Cachexia in Patients With Advanced Cancer. *JCSM Commun.* **2025**, *8*, e70001. [CrossRef]
46. Dwarkasing, J.T.; Boekschoten, M.V.; Argiles, J.M.; van Dijk, M.; Busquets, S.; Penna, F.; Toledo, M.; Laviano, A.; Witkamp, R.F.; van Norren, K. Differences in food intake of tumour-bearing cachectic mice are associated with hypothalamic serotonin signalling. *J. Cachexia Sarcopenia Muscle* **2015**, *6*, 84–94. [CrossRef] [PubMed] [PubMed Central]

Disclaimer/Publisher's Note: The statements, opinions and data contained in all publications are solely those of the individual author(s) and contributor(s) and not of MDPI and/or the editor(s). MDPI and/or the editor(s) disclaim responsibility for any injury to people or property resulting from any ideas, methods, instructions or products referred to in the content.